REPORT - 419 JUNE 1969

CSL COORDINATED SCIENCE LABORATORY

ONE-ELECTRON AND PHONON-ASSISTED TUNNELING IN N-Ge SCHOTTKY BARRIERS

L.C. DAVIS
F. STEINRISSER

UNIVERSITY OF ILLINOIS - URBANA, ILLINOIS

ONE-ELECTRON AND PHONON-ASSISTED TUNNELING IN N-Ge SCHOTTKY BARRIERS

L. C. Davis and F. Steinrisser
Department of Physics and Coordinated Science Laboratory
University of Illinois, Urbana, Illinois
June, 1969

This work was supported in part by the National Aeronautics and Space Administration under grant NsG 228-62, by the Joint Services Electronics Program (U.S. Army, U.S. Navy, and U.S. Air Force) under Contract DAAB-07-67-C-0199, and by the U.S. Army Research Office (Durham) under Contract DA-31-124-ARO(D)-114.

One-Electron and Phonon-Assisted Tunneling in N-Ge Schottky Barriers*

L. C. Davis+ and F. Steinrisser**

Department of Physics and Coordinated Science Laboratory

University of Illinois, Urbana, Illinois

* This work was supported in part by the National Aeronautics and Space Administration under grant NsG 228-62, by the Joint Services Electronics Program, Army contract DAAB-07-67-C0199, and by the U. S. Army Research Office (Durham) under contract DA-31-124-ARO(D)-114.

+ National Science Foundation Post-doctoral Fellow.

**Present Address: Ford Scientific Labs, Dearborn, Michigan, 48121

Abstract

The experimental tunneling conductance of metal-Ge contacts is compared to the predictions of the one-electron Schottky-barrier model in which all parameters are determined from experiments other than tunneling. Agreement is found in the magnitude and the shape of conductance vs bias curves for vacuum-cleaved, Sb-doped Ge units. The qualitative features of the As-doped units are also in agreement, but a discrepancy in magnitude exists. Substantially larger conductance is found in air-cleaved junctions than in vacuum-cleaved junctions. Capacitance measurements reveal that the barrier height for air-cleaved junctions is V_b=0.51V whereas V_b=0.63V for vacuum-cleaved junctions. Pronounced step increases in the conductance due to phonon-assisted tunneling occur at $eV = \pm\hbar\omega$ where $\hbar\omega$ is the energy of a Ge phonon at the Brillouin zone boundary along the <111> direction. Structure is clearly observed at all four phonon energies (TA,LA,LO,TO). The magnitude of the LA phonon-assisted tunneling is accounted for in a theoretical calculation based upon a mechanism suggested by Kleinman to explain similar phenomena in Ge p-n junctions. The strength of the TA and LO phonon-assisted tunneling also appear to be in reasonable agreement with qualitative considerations, but the observed TO phonon-assisted tunneling is stronger than expected.

I. Introduction

A calculation of the tunneling conductance as a function of bias voltage for a metal-semiconductor junction has been given by Conley, Duke, Mahan, and Tiemann (CDMT)[1]. This calculation was based upon the Schottky model with a parabolic potential for the barrier. Specular reflection at the metal-semiconductor

interface was assumed. The mobile charge carriers of the highly doped, degenerate n-type semiconductor electrode were taken to behave as a free-electron gas with Fermi energy $e\mu_F$ (Fermi level $e\mu_F$ above conduction band edge) at T = 0^oK and an effective mass m_c^*. The first comparison of experimental data to the CDMT calculation was given by Conley and Tiemann.[2] They found favorable agreement (but with some discrepancies) for chemically prepared diodes made from degenerate n-type Ge and either Au or In as the metal electrode. Subsequently, it was shown[3] that the technique of evaporation of metal electrodes on vacuum-cleaved, Sb-doped Ge surfaces gave greatly improved agreement with theory. It was concluded that the absolute magnitude, as well as the shape of the experimental curve was adequately described by the one-electron theory of Schottky-barrier tunneling with all parameters in the calculation determined from experiments other than tunneling.[3] The agreement in As-doped Ge units, however, was not as good as in Sb-doped units.

The purpose of the first part of this paper is to discuss the comparison of Sb-doped units to theory with a more accurate measurement of the carrier density, to present data for As-doped units, and to describe the effects of air cleavage on both the tunneling conductance and the barrier heights (as determined from capacitance measurements).

In the second part of the paper, we discuss the step increases in the conductance due to strong phonon-assisted tunneling observed in both Sb-doped and As-doped metal-Ge junctions. This inelastic tunneling process involves the emission of Ge phonons of all four branches (transverse acoustic = TA, longitudinal acoustic = LA, longitudinal optic = LO, transverse optic = TO) at the Brillouin zone-bondary along the <111> axis. These are the same phonons

as observed in Sb-doped Ge p-n junctions[4] where the emission of zone-boundary phonons along the <111> axis is required for momentum conservation in an indirect diode (in the absence of appreciable impurity scattering which obscures the phonon effects in As-doped Ge p-n junctions[5]). In the metal-semiconductor contact, we find that the same momentum conservation rule applies to electrons with small $k_{\parallel}$ in the metal. A calculation of the strength of the LA phonon-assisted tunneling in the metal-semiconductor contact based upon a modification of Kleinman's theory for indirect p-n junctions is described in sec. 4. As previously noted[3], the Kleinman mechanism is a two-step process of an electron first tunneling from the metal (in reverse bias) into an evanescent state associated with the electronic spectrum at Γ_2' in the Ge Brillouin zone, and then emitting a phonon and being scattered into a current-carrying state at L_1.

II. Experimental Technique

Contact preparation. Single crystal bars of n-type Ge doped to an impurity concentration of approximately $7 \times 10^{18}/cm^3$ with As or Sb were cut with the long axis in the <100> direction. The sample size was 10x4x2 mm. After being cut, the samples were etched in CP-4.

Ohmic contacts were attached to the bars by soldering copper wires with an In-Sn solder to them. Bars which had two such contacts were checked at $4.2^{\circ}K$. The contacts were ohmic and exhibited a very low resistance.

Tunneling contacts were made by cleaving the bars in a vacuum of 1×10^{-7} torr after scribing them in the middle with a diamond. A few seconds after cleavage, a stainless steel mask was brought close to the (100) cleavage plane. A shutter between the evaporation source and the sample was opened. 99.999% pure

In or 99.99% pure Pb was evaporated from alumina coated wire baskets. The evaporation was started about one minute before cleavage such that the evaporation rate had stabilized at 50 Å/sec at the time of cleavage. Dots of 2.5×10^{-4} cm^2 and 5×10^{-5} cm^2 area were evaporated to a thickness of ~5000 Å as monitored by a quartz crystal deposition monitor.

Contacts to the In or Pb dots were made by pressing a freshly cut In wire tip into a dot located on a good cleavage area. Cold welding produced satisfactory electrical and mechanical contacts.[1]

Low temperature measurements. Tunneling measurements were performed in a helium immersion dewar. Temperatures below 4.2°K were obtained by pumping on the liquid helium. The lowest temperature was 1.8°K. A calibrated Ge thermometer was used for temperature measurements. A Cartesian manostat inserted in the helium pump line kept the temperature constant to better than 1%.

The occurrence of tunneling was confirmed by the observation of the superconducting energy gap in the contact metal below its critical temperature, i.e., 3.4°K for In and 7.2°K for Pb, respectively.

Electronics. Conductance, dI/dV, and second derivative, d^2I/dV^2, measurements were made according to standard techniques.[7,8] Fig. 1 shows schematically the setup which is approximately the same as the one shown in Fig. 6 of Reference 4. The dc source which could be swept electronically from -6 V to +6 V was a transistorized power supply fed by two wet cells. The dc source was shunted by a resistor R_{dc} of 2Ω in series with a resistor R_s of 1Ω or 0.1Ω. The ac modulation at a frequency f = 1000 cps was supplied by an audio generator. It was shunted by a variable resistor $R_{ac} < 1$ kΩ in series with R_s. R_{dc} and R_{ac} serve to decouple dc and ac sources from each other.

R_s determined the source resistance seen by the junction. R_s assured a constant ac level for varying junction resistance as long as it was chosen much smaller than the junction resistance.

The dc and ac voltage developed across R_s was applied through a sampling resistor R to the tunneling junction. The ac current I(f) and I(2f) at the frequencies f and 2f, respectively, flowing through R was converted into a voltage which was fed through a capacitor C into a transformer T. The voltage was amplified and detected by a lock-in detector.

According to Reference 4, the currents I(f) and I(2f) are related to dI/dV and d^2I/dV^2 as follows:

$$I(f) = \frac{dI}{dV}\left(1 + \frac{dI}{dV}R\right)^{-1} V_{ac} + \text{const}\,\frac{d^3I}{dV^3} V_{ac}^{\,3}, \tag{2.1}$$

$$I(2f) = (2)^{-\frac{3}{2}}\frac{d^2I}{dV^2}\left(1 + \frac{dI}{dV}R\right)^{-3} V_{ac}^{\,2} + \text{const}\,\frac{d^4I}{dV^4} V_{ac}^{\,4}. \tag{2.2}$$

In this case, R is the value of the sampling resistor [R in Fig. 1] plus the lead resistance, and V_{ac} is the ac amplitude measured across R_s.

The values of R were chosen such that $(dI/dV)\,R \ll 1$. V_{ac} was small enough that the contributions due to higher order terms were negligible. Consequently, dI/dV and d^2I/dV^2 were proportional to I(f) and I(2f), respectively. Calibration of dI/dV was done by replacing the sample by a precision resistance decade.

Barrier heights. The barrier height V_b was determined by measuring junction capacitance C vs bias voltage V at 77°K with a Boonton 33A rf admittance bridge.

The frequency was 1 MHz, the modulation amplitude was 5 mV. The capacitance C of a metal-degenerate semiconductor contact is given by

$$C = A\left[\frac{e^2\epsilon_s n_D}{8\pi(eV_b+3/5e\mu_F- eV)}\right]^{\frac{1}{2}} \qquad (2.3)$$

with A = junction area, e = electron charge, ϵ_s = static dielectric constant of the semiconductor, n_D = number of free carriers per unit volume, V_b = barrier height, μ_F = Fermi degeneracy of the semiconductor, and V = applied bias. In this paper the sign convention for V is that $V > 0$ when the metal is positive with respect to the n-type semiconductor which is opposite to the sign convention in Reference 3.

By plotting $1/C^2$ vs V, one obtains a straight line whose intersection with the V-axis determines $eV_b + 3/5\ e\mu_F$. For vacuum cleaved contacts, it was found that $V_b = 0.63 \pm 0.03$ V. V_b was found to be independent of the contact metal (In or Pb) and independent of the dopant of the semiconductor (Sb or As). For air cleaved junctions, the value of V_b was found to be 0.51 ± 0.03 V. Within experimental error, the junction capacitance values at fixed bias voltages agreed with eq. (2.3). Curves of $1/C^2$ vs. V were slightly concave but they could be closely approximated by straight lines. The largest uncertainty was in the determination of the junction area, this uncertainty amounting to about 20%. This was due to poorly defined edges of the evaporated dots caused by the separation of the evaporation mask from the sample during evaporation and by the finite size of the evaporation source.

Carrier concentrations. Carrier concentrations were determined by measuring Hall coefficients on clover-leaf samples 1/8 inch in diameter. The

Hall samples were cut from the tunneling bars. Measurements were performed at room temperature and at 77°K and gave identical results within experimental error ($\sim$ 1%). Bulk resistivities were also obtained from these measurements. Bulk resistivities and Hall coefficients agree well with the published data of Spitzer et. al.[10]

III. Experimental results and comparison with theory

A. Conductance vs voltage curves

In Reference 2, differential resistance dV/dI vs V curves are displayed which show an order-of-magnitude agreement with the theory developed in Reference 1. The agreement in curve shape, absolute value, and position of the resistance maximum was considered to be satisfactory. The discrepancies observed were attributed to shortcomings in the theory such as the omission of band tailing.[2] Our results indicate that improved diode fabrication techniques give much better agreement between experiment and the theory of Reference 1, particularly for Sb-doped germanium. The agreement in the case of As-doped Ge, however, is not as good.

Results for Sb-doped germanium. In Fig. 2, conductance dI/dV vs voltage curves at T = 4.2°K are displayed for an indium contact on Sb-doped Ge [solid line]. This is one typical curve out of 12 curves of which the high and low extremes and the most commonly observed curves were displayed in Fig. 1 of Reference 3. The dashed curve in Fig. 2 is a theoretical calculation based on the CDMT theory.[1] The following experimentally determined parameters were used in the calculation: carrier density $n_D = (6.7 \pm 0.1) \times 10^{18}/cm^3$, (11) barrier height $V_b = 0.63 \pm 0.03$ V, and junction area $A = (2.5 \pm 0.5) \times 10^{-4}$

cm^2. The tunneling mass was assumed to be 0.12 m_o which is the value for the tunneling mass in the 100 direction.[1] [Eq.(7) of Ref. 1 was used with corrections to the asymptotic expansions of the parabolic cylinder functions].

The agreement between theory and experiment in probably fortuitous considering the experimental uncertainties and the approximations made in the theory. However, the following appear to be approximations adequate for the description of the Sb-doped Ge units measured in this investigation. (1) The current transfer mechanism is that appropriate to electrons tunneling through an average electrostatic potential which is parabolic, and, at least for doping levels $n_D \sim 7 \times 10^{18}$ cm^{-3}, fluctuations from this average barrier potential are not important. (2) Specular reflection occurs at the metal-semiconductor interface. (3) The energy levels of the electrons in highly doped n-Ge contributing to the tunneling current are given by $\frac{\hbar^2 k^2}{2m_c^*}$ where m_c^* is the effective mass of the intrinsic conduction band (or the appropriate generalization for ellipsoidal energy surfaces). This last assumption implies that the Fermi level for n-Ge should be at $e\mu_F = \frac{\hbar^2}{2m_d^*}(3\pi^2 n_D/4)^{2/3}$ above the conduction band edge in the absense of carrier freeze-out (m_d^* is the density-of-states mass = $0.22m_o$ for n-Ge). The presence of the sharp minimum in the experimental data at a bias equal to the calculated μ_F (the sharpness of the minimum is due to the improved diode fabrication) is a direct confirmation of this idea. No evidence of a component in the conductance due to band tailing was found.

Results for As-doped germanium. Results for vacuum- and air-cleaved samples and a comparison with theory are displayed in Fig. 3. The curve for a vacuum-cleaved sample represents one typical curve out of a total of 10. The curve denoted "air cleaved" represents one out of two almost identical curves.

The results shown in Fig. 3 for air- and vacuum-cleaved contacts were obtained from the same single-crystal bar.

The theoretical curves were calculated with the following measured parameters: carrier density $n_D = (5.1 \pm 0.1) \times 10^{18}/cm^3$, barrier heights $V_b = 0.63 \pm 0.03$ V and 0.51 ± 0.03 V for vacuum- and air-cleaved junctions, respectively. The junctions area was $(2.5 \pm 0.5) \times 10^{-4} cm^2$. The value, $0.12\ m_o$, was used for the tunneling mass for the calculations.

At present it is not known why the agreement between experiment and theory in absolute value of the conductance vs voltage curves is not as good for vacuum-cleaved As-doped junctions as it is for Sb-doped ones. However, it should be pointed out that the qualitative features of the vacuum-cleaved As-doped Ge data are in good agreement with the theory, and considering the experimental uncertainties in the parameters and the scattering properties of As impurities[5], the discrepancies in absolute value are not too surprising.

B. Phonon-assisted tunneling

In all junctions made with Sb- and As-doped Ge which were fabricated with the vacuum-cleavage technique, strong, sharp, step increases in the conductance vs bias curves were observed at bias voltages corresponding to the four zone-boundary phonon energies in the <111> direction.[4] Air-cleaved junctions showed the same type of structure, but very weakly. The chemically prepared units of Reference 2 showed no such structure.

In Fig. 4, dI/dV and d^2I/dV^2 vs bias curves are shown for an In contact on vacuum cleaved As-doped Ge. The temperature was 2^oK. Identical structure with nearly the same strength was also found in Sb-doped units. The magnitude of the conductance change at $eV = \pm \hbar \omega_{LA}$ was approximately $10^{-4}\ \Omega$ for both Sb

and As-doped vacuum-cleaved units. As is shown in sec. 4, a conductance increase of this magnitude is expected for the Kleinman mechanism[6] of LA phonon-assisted tunneling in metal-semiconductor contacts.

IV. LA Phonon-assisted tunneling in n-Ge

In this section we calculate the change $\Delta(\frac{dI}{dV})$ in the conductance at $eV = \pm \hbar\omega_{LA}$, where $\hbar\omega_{LA}$ is the energy of the longitudinal acoustic phonon (LA) of momentum $\underline{q} = \frac{\pi}{a}(1,1,1)$. These step increases at $\pm \hbar\omega_{LA}$ in the conductance are attributed to a mechanism suggested by Kleinman to explain similar effects in p-n tunnel junctions. For our calculation, there are two important differences between p-n junctions and metal-semiconductor junctions. (1) The electrostatic potential in a p-n junction can be treated as linear in the junction region, whereas in the metal-semiconductor contact, the electrostatic potential near the metal-semiconductor interface is parabolic to a good approximation. (2) The basis functions in a p-n junction are just the complete set of Bloch states in a semiconductor. In the metal-semiconductor contact, we must mix metal and semiconductor basis functions, assuming some type of matching procedure at the interface of the metal and semiconductor.

In Fig. 5, we show a schematic drawing of the band structure of Ge. For n-Ge at $T = 0^{o}K$, the valence bands are filled and the L_1 conduction band is filled up to an energy $e\mu_F$ above E_{Lc} (for 7×10^{18} cm^{-3} donors in Ge, $\mu_F = 24mV$). The subsidary Γ_2' conduction band is empty. The selection rules for phonon emission[12] are also shown in Fig. 5. The important transition for LA phonons is $\Gamma_2' \leftrightarrow L_1$. The observation of LA phonon emission in the tunneling conductance of our n-Ge units is qualitatively explained as follows.

Consider an applied bias such that electrons are injected from the metal electrode into the Ge electrode ($V<0$, i.e., metal negative relative to Ge). Most of the current flows by the direct channel in which no phonon emission occurs (Fig. 6a). For tunneling into the (100) face, the four ellipsoids associated with the L_1 conduction band are equivalent, so only one is considered. The metal Fermi surface is large enough to allow direct tunneling without violation of the $\underline{k}_{\parallel}$-conservation rule (specular reflection). This type of tunneling is described by the CDMT theory.[1]

Another channel for tunneling is the phonon-assisted tunneling which is a two-step process. (Step 1) The first step is the injection of electrons from near the forward direction ($\underline{k}_{\parallel} \approx 0$) on the metal Fermi surface into states associated with the Γ_2' conduction band; for the bias voltages of interest, these states are of an energy below the Γ_2' conduction band edge $E_{\Gamma c}$, so these states are decaying or evanescent states in the semiconductor (Fig. 6b). The important point made by Kleinman[6] is that this exponential tail extends well beyond the junction region into the semiconductor $x > d$ (where d is the width of the space-change region) and is primarily of the Γ_2' symmetry. Hence, there is a rather large region for interaction with phonons. The tunneling channel for the electron is completed by the emission of a LA phonon of wavevector $\underline{q} \simeq \frac{-\pi}{a}(1,1,1)$ allowing the electron to make a transition from the state of Γ_2' symmetry to a current-carrying state of symmetry L_1 at $\underline{k} = \frac{\pi}{a}(1,1,1)$ (Step 2). A similar two-step process occurs when the Ge electrode is biased negative relative to the metal.

It is clear from the conservation of energy that the LA phonon assisted tunneling can only occur when $eV \geq \hbar\omega_{LA}$ or $eV \leq -\hbar\omega_{LA}$. For example, when electrons are injected from the metal into the Ge, the condition $eV \geq \hbar\omega_{LA}$ must

hold if an electron is to emit a phonon of energy $\hbar\omega_{LA}$ and make a transition to an unoccupied state above the Fermi level in the Ge electrode.

Let us now calculate quantitatively the change $\Delta(\frac{dI}{dV})$ in the conductance at $eV = \pm \hbar\omega_{LA}$. For simplicity, we follow Kleinman[6] and calculate only that contribution which comes from the interaction occuring in the region $x > d$. The contribution from the region $x < d$ should be smaller than that for $x > d$ because the symmetry of the wavefunction is predominantly hole-like near $x = 0$ (Γ_{25}' symmetry).

The Bloch states for $\underline{k}_r$ near $\underline{k}_o = \frac{\pi}{a}(1,1,1)$ with energy $E_{\underline{k}r}$ near E_{Lc} (energy of L_1 state at $\underline{k}_o$) can be written as[6,13]

$$\Psi_{\underline{k}r} = e^{i(\underline{k}_r - \underline{k}_o)\cdot\underline{r}}\, u_{Lc}(\underline{r}),\ x > d, \tag{4.1}$$

where $u_{Lc}(\underline{r})$ is the Bloch function at $\underline{k}_o$ with L_1 symmetry. The states of symmetry Γ_2' associated with $\underline{k} = 0$ and energy $E_{\underline{k}\ell}$ near $E_{\Gamma c}$ are written as[6, 13]

$$\Psi_{\underline{k}\ell} = \beta(x)\, e^{ik_{\ell\|}\cdot\underline{r}}\, u_{\Gamma c}(\underline{r}),\ x > 0. \tag{4.2}$$

$u_{\Gamma c}(\underline{r})$ is the Bloch function at $\underline{k} = 0$ with Γ_2' symmetry and energy $E_{\Gamma c}$. The envelope function $\beta(x)$ is a solution to ($x>0$)

$$-\frac{\hbar^2}{2m_{\Gamma c}}\frac{d^2\beta}{dx^2} + V(x)\,\beta = (E_{\underline{k}\ell} - E_{\Gamma c} - \frac{\hbar^2 k_{\ell\|}^2}{2m_{\Gamma c}})\,\beta\,. \tag{4.3}$$

The effective mass of the Γ_2' conduction band is denoted by $m_{\Gamma c}$ and the electrostatic potential[9] is

$$V(x) = \begin{cases} \dfrac{2\pi e^2 n_D}{\epsilon_s}(x-d)^2, & d > x > 0 \\ 0, & x > d. \end{cases} \tag{4.4}$$

The number of donors per unit volume is n_D, the static dielectric constant of the semiconductor is ϵ_s, and d is given by (in the parabolic potential approximation)[9]

$$eV_b + e\mu_F - eV = \frac{2\pi e^2 n_D}{\epsilon_s} d^2, \tag{4.5a}$$

$$d = \left[\frac{\epsilon_s}{2\pi e n_D} (V_b + \mu_F - V)\right]^{\frac{1}{2}}, \tag{4.5b}$$

where V_b is the barrier height.

Eq. (4.3) is valid if $eV_b \lesssim \frac{1}{2} E_g$ where E_g is the direct gap. Since eV_b = .63eV and E_g = .95eV, we see that (4.3) will not be valid for x near 0. We will account for this in our final expression for $\Delta(\frac{dI}{dV})$ by estimating the influence of the valence band with a two-band model. However, for simplicity let us initially assume that eq. (4.3) is valid for all $x > 0$.

To completely specify $\beta(x)$, we must match $\beta(x)$ at x = 0 to the envelope function in the metal which is of the form

$$\beta(x) = 2\sqrt{\sin}\,(k_{\ell x} x + \delta), \; x < 0, \tag{4.6}$$

where δ is a phase angle and $k_{\ell x} \simeq k_F$, the metal Fermi radius, for the states of interest. We require continuity of $\beta(x)$ and $\frac{1}{m^*}\frac{d\beta}{dx}$ at x = 0[14]. We also assume $\underline{k}_{\|}$ conservation (specular reflection).

The notation employed is that $\underline{k_r}$ represents the L_1 current carrying states and $\underline{k_\ell}$ the metal - Γ_2' states.

We note that for $x > d$,

$$\beta(x) = \beta(d)\, e^{-K_{\Gamma c}(x-d)}, \tag{4.7}$$

where

$$K_{\Gamma c} = \left[k_{\ell\|}^2 + \frac{2m_{\Gamma c}}{\hbar^2}(E_{\Gamma c} - E_{\underline{k\ell}})\right]^{\frac{1}{2}}. \tag{4.8}$$

For the calculation of $\Delta(\frac{dI}{dV})$ we will be interested in the case ($eV = \pm \hbar\omega_{LA}$)

$$E_{k\ell} = -eV + e\mu_F. \tag{4.9}$$

Following CDMT[1], we write $\beta(x)$ as

$$\beta(x) = A\, U(a,\eta) + B\, V(a,\eta), \tag{4.10}$$

where

$$a = \lambda^2\left[k_{\ell\|}^2 + \frac{2m_{\Gamma c}}{\hbar^2}\,(E_{\Gamma c} - E_{k\ell})\right] = \lambda^2 K_{\Gamma c}^2, \tag{4.11a}$$

$$\lambda = \left[\frac{\hbar^2 \epsilon_s}{16\pi\, m_{\Gamma c} e^2 n_D}\right]^{\frac{1}{4}}, \tag{4.11b}$$

$$\eta = (d-x)/\lambda. \tag{4.11c}$$

A and B are constants to be determined by matching $\beta(x)$ at $x = 0$ and $x = d$, and $U(a,\eta)$ and $V(a,\eta)$ are parabolic cylindrical functions.[15] $V(a,\eta)$ is the exponentially increasing function as $\eta \to \infty$, and $U(a,\eta)$ is the exponentially decreasing function as $\eta \to \infty$.

Applying the matching conditions and neglecting $U(a,\eta_d)$ compared to $V(a,\eta_d)$, where

$$\eta_d = d/\lambda, \tag{4.12}$$

we find

$$|\beta(d)|^2 = \frac{4\,(2\pi)^{\frac{1}{2}}\,\lambda K(0)\,\exp\,(-2\int_o^d K dx)}{\Gamma(\frac{1}{2} + a)\left[1 + \left[\frac{m_o K(0)}{m_{\Gamma c} k_F}\right]^2\right]\left[U'(a,o) - a^{\frac{1}{2}}\, U(a,o)\right]^2}, \tag{4.13}$$

where

$$K^2(x) = k_{\ell\|}^2 + \frac{2m_{\Gamma c}}{\hbar^2}\left[E_{\Gamma c} - E_{k\ell} + V(x)\right], \tag{4.14}$$

and the metal electron mass is taken to be the free electron mass, m_o.

We have made use of Darwin's asymptotic expansion[15] for $V(a,\eta)$ in eq. (4.14) in place of the asymptotic form used in CDMT[1] because the former is more closely related to the WKB approximation.

To take account of the influence of the valence band and the breakdown of eq. (4.3) near $x = 0$, we replace $K(x)$ above with the expression obtained for a trajectory in a two-band model[9] (for $k_{\|} = 0$).

$$K(x) = \left[\frac{2m^*}{\hbar^2 E_g} (V(x) - E_{\underline{k\ell}} + E_{\Gamma c}) (E_g - V(x) + E_{\underline{k\ell}} - E_{\Gamma c})\right]^{\frac{1}{2}}, \tag{4.15a}$$

$$\text{where } \frac{1}{m^*} = \frac{1}{2} \left(\frac{1}{m_{\Gamma c}} + \frac{1}{m_v}\right), \tag{4.15b}$$

The effective mass of the light hole valence band is m_v. We find

$$\int_0^d K dx = \frac{C}{3} \left[(\zeta - 2\epsilon)\, E(\varphi,k) + \epsilon\, F(\varphi,k) + (\alpha + 3\epsilon - \zeta) \sqrt{\frac{\alpha(\zeta - \epsilon - \alpha)}{\zeta\,(\alpha + \epsilon)}} \right], \tag{4.16a}$$

where

$$\alpha = (V_b + \mu_F - eV)/\mu_F, \qquad \zeta = E_g/\mu_F,$$

$$\epsilon = (E_{\Gamma c} - E_{\underline{k\ell}})/\mu_F, \qquad \sin\varphi = \sqrt{\frac{\alpha\zeta}{(\zeta - \epsilon)\,(\alpha + \epsilon)}}, \tag{4.16b}$$

$$C = \mu_F/E_o, \qquad k = \sqrt{\frac{\zeta - \epsilon}{s}}.$$

$$E_o = \left[\frac{\hbar^2 \pi\, e^2\, n_D}{m^*\, \epsilon_s}\right]^{\frac{1}{2}},$$

E and F are incomplete elliptic integrals. We note that our result differs from that of Conley and Mahan[9] because no turning point occurs between $0 \leq x \leq d$.

Let us now calculate the transition rate for a transition from $\Psi_{\underline{k\ell}}$ to $\Psi_{\underline{kr}}$ with the emission of a LA phonon of wavevector $\underline{q}$,

$$P_{\underline{k\ell},\underline{kr}}(\underline{q}) = \frac{2\pi}{\hbar} \left| < \Psi_{\underline{k\ell}} \left| H_{\text{el-ph}} (q) \right| \Psi_{\underline{kr}} > \right|^2 \delta(E_{\underline{k\ell}} - E_{\underline{kr}} - \hbar\omega_{LA}), \tag{4.17a}$$

$$= \frac{2\pi}{\hbar} \left| \beta(d) \right|^2 M^2_{LA} \left| \int_d^\infty dx\, e^{-K_{\Gamma c}(x-d)}\, e^{iq_x x}\, e^{ik_{rx}x} \right|^2 \delta_{k_{\ell\|},\, q_\| + k_{r\|}} \times \delta(E_{\underline{k\ell}} - E_{\underline{kr}} - \hbar\omega_{LA}), \tag{4.17b}$$

$$= \frac{2\pi}{\hbar} \frac{\left|\beta(d)\right|^2 M^2_{LA}}{(q_x + k_{rx})^2 + K^2_{\Gamma c}}\, \delta_{k_{\ell\|},\, q_\| + k_{r\|}}\, \delta(E_{\underline{k\ell}} - E_{\underline{kr}} - \hbar\omega_{LA}). \tag{4.17c}$$

The matrix element M_{LA} is defined as

$$M_{LA} = \langle u_{\Gamma c} \left| H_{\text{el-ph}} (\underline{k}_o) \right| u_{Lc} \rangle. \tag{4.18}$$

We use normalization in a unit volume, neglect dispersion in the phonon energy $\hbar\omega_{LA}$, and consider only the contribution from $x > d$.

To be completely rigorous, we should have taken the L_1 states to be standing waves in place of running waves and we should have taken account of the boundary in the phonon mode description. To the extent that we average over $\underline{k}$ and $\underline{q}$ in calculating the conductance, such essentially interference effects should vanish.

For $V < 0$, the current due to this mechanism at $T = 0^{\circ}K$ is

$$I = -8eA \sum_{\underline{k}_\ell,\, \underline{k}_r,\, \underline{q}} P_{\underline{k\ell},\, \underline{kr}}(\underline{q})\, f(\underline{k}_\ell) \left[1 - f(\underline{k}_r)\right], \tag{4.19}$$

where $f(\underline{k})$ is the Fermi function and A is the area of the junction. The factor 8 arises from the 2 spin directions and the 4 conduction band minima in Ge.

Performing the sum over $\underline{q}$, we find

$$\sum_{\underline{q}} P_{\underline{k\ell},\, \underline{kr}}(\underline{q}) = \frac{2\pi}{\hbar} \left|\beta(d)\right|^2 M^2_{LA} \left(\frac{1}{2K_{\Gamma c}}\right) \delta(E_{\underline{k\ell}} - E_{\underline{kr}} - \hbar\omega_{LA}). \tag{4.20}$$

We see that $\sum_{\underline{q}} P_{\underline{k\ell},\,\underline{kr}}(\underline{q})$ depends on the variables $E_{\underline{k\ell}}$, $E_{\underline{kr}}$, and $k_{\underline{\ell\|}}$ [$\beta(d)$ and $K_{\Gamma c}$ depend upon $k_{\underline{\ell\|}}$], so we write

$$I = -\frac{8eA\,M^2_{LA}}{\hbar^2 v_F}\int dE_{\underline{k\ell}}\, f(E_{\underline{k\ell}} + eV - e\mu_F)\int dE_{\underline{kr}}\,\rho(E_{\underline{kr}})\left[1 - f(E_{\underline{kr}} - e\mu_F)\right]$$

$$X\,\delta(E_{\underline{k\ell}} - E_{\underline{kr}} - \hbar\omega_{LA})\int \frac{d^2k_{\underline{\ell\|}}}{(2\pi)^2}\,\frac{|\beta(d)|^2}{K_{\Gamma c}}, \qquad (4.21)$$

where $\rho(E)$ is the Ge density of states for one spin band and one conduction band minimum at L_1. The energy variable $E_{\underline{k\ell}}$ is the total energy, including potential energy, measured relative to the L_1 conduction band edge. The Fermi velocity of the metal is $v_F = \frac{\hbar k_F}{m_o}$.

Doing the $E_{\underline{kr}}$ integration, we find

$$I = -\frac{8eA\,M^2_{LA}}{\hbar^2 v_F}\int dE_{\underline{k\ell}}\,\rho(E_{\underline{k\ell}} - \hbar\omega_{LA})\,f(E_{\underline{k\ell}} + eV - e\mu_F)$$

$$X\left[1 - f(E_{\underline{k\ell}} - \hbar\omega_{LA} - e\mu_F)\right]\int \frac{d^2k_{\underline{\ell\|}}}{(2\pi)^2}\,\frac{|\beta(d)|^2}{K_{\Gamma c}}. \qquad (4.22)$$

We are interested in the conductance, dI/dV, which is given by

$$\frac{dI}{dV} = \frac{8e^2A\,M^2_{LA}}{\hbar^2 v_F}\,\rho(e\mu_F - eV - \hbar\omega_{LA})\left[1 - f(-eV-\hbar\omega_{LA})\right]\int \frac{d^2k_{\underline{\ell\|}}}{(2\pi)^2}\,\frac{|\beta(d)|^2}{K_{\Gamma c}}. \qquad (4.23)$$

In eq. (4.23) we have taken a derivative of the Fermi function only. The $E_{\underline{k\ell}}$ variable in the expressions for $|\beta(d)|^2$ and $K_{\Gamma c}$ (eqs. (4.8) and (4.13)) is evaluated at $e\mu_F - eV$. The $k_{\underline{\ell\|}}$ integration can be extended to infinity.

We see from eq. (4.23) that dI/dV vanishes for $-\hbar\omega_{LA} < eV < 0$, and has a step increase at $eV = -\hbar\omega_{LA}$ (see Fig. 7)

$$\Delta\left(\frac{dI}{dV}\right) = \frac{8e^2 A M_{LA}^2 \rho(e\mu_F)}{\hbar^2 v_F} \int \frac{d^2k_{\ell\|}}{(2\pi)^2} \frac{|\beta(d)|^2}{K_{\Gamma c}}, \tag{4.24}$$

where $E_{k\ell}$ is evaluated at $e\mu_F + \hbar\omega_{LA}$. Similarly, for $V>0$, we find dI/dV vanishes for $0<eV<\hbar\omega_{LA}$ and has a step increase at $eV = \hbar\omega_{LA}$ given by eq. (4.24) with $E_{k\ell}$ evaluated at $e\mu_F - \hbar\omega_{LA}$.

The most important $k_{\ell\|}$ dependence of $\frac{|\beta(d)|^2}{K_{\Gamma c}}$ is in the WKB exponential $\int_o^d K(k_{\ell\|}, x)\, dx$ (previously we have suppressed the variable $k_{\ell\|}$ in K(x)) where

$$K(k_{\ell\|}, x) = \sqrt{K^2(x) + k_{\ell\|}^2}\ . \tag{4.25}$$

In eq. (4.25) K(x) is given by eq. (4.15). We estimate the $k_{\ell\|}$ integral in eq. (4.24) by expanding the WKB exponent to order $k_{\ell\|}^2$ and neglecting all other $k_{\ell\|}$ dependences. Hence, to a reasonable approximation

$$\int \frac{d^2k_{\ell\|}}{(2\pi)^2} \frac{|\beta(d)|^2}{K_{\Gamma c}} \simeq \frac{k_a^2}{4\pi} \left(\frac{|\beta(d)|^2}{K_{\Gamma c}}\right)_o, \tag{4.26a}$$

where

$$\frac{1}{k_a^2} = \int_o^d K^{-1}(x)\, dx\ , \tag{4.26b}$$

and

$$\left(\frac{|\beta(d)|^2}{K_{\Gamma c}}\right)_o = \left(\frac{|\beta(d)|^2}{K_{\Gamma c}}\right)_{k_{\ell\|}=0}. \tag{4.26c}$$

From eq. (4.15), we find

$$\frac{1}{k_a^2} = \frac{\hbar^2 F(\varphi,k)}{2m^* E_o} , \tag{4.27}$$

where the definitions in eq. (4.16b) apply.

Hence, we find that the step increase in the conductance at $eV = \pm \hbar\omega_{LA}$ is given by

$$\Delta\left(\frac{dI}{dV}\right) = \frac{2e^2 A M_{LA}^2 \rho(e\mu_F) k_a^2}{\pi \hbar^2 v_F} \left(\frac{|\beta(d)|}{K_{\Gamma c}}^2\right)_o . \tag{4.28}$$

Using the parameters listed in table I[16], we find that (ignoring small differences between forward and reverse bias due to the changing space charge region)

$$\Delta\left(\frac{dI}{dV}\right) \simeq 10^{-4}\ \Omega^{-1}, \tag{4.29}$$

which is in order-of-magnitude agreement with the experimental data for vacuum-cleaved Sb-doped and Ge units. [The predicted size of the effect for vacuum-cleaved As-doped units ($n_D = 5.1 \times 10^{18}/cm^3$) is an order of magnitude lower than that observed, which is also the case for the background conductance in Fig. 3.] Since the background conductance $\sim 10^{-3}\Omega^{-1}$, the step increases for LA phonon-assisted tunneling are approximately 10% of the background which makes them easily detectable.

Table I. Parameters for LA Phonon-Assisted Tunneling

$n_D = 7 \times 10^{18}$ cm^{-3}	$A = 2.5 \times 10^{-4}$ cm^2
$\epsilon_s = 16$	$\hbar\omega_{LA} = 28$meV
$m_{\Gamma c} = .034\ m_o$	$M^2_{LA} = 4.3 \times 10^{-49}$ erg^2 cm^3
$m_v = .044\ m_o$	$v_F = 1.7 \times 10^8$ cm/sec
$m^* = .038\ m_o$	$E_{\Gamma c} - E_{Lc} = 0.154$ eV
$\mu_F = 24$mV	$E_{Lc} - E_{Lv} = 2.36$ eV
$V_b = 0.63$ B	
$E_g = 0.91$ eV (Direct gap)	

V. Phonon-Assisted Tunneling Due to TA, LO, and TO Phonon Emission

We have given a detailed analysis of only the LA phonon-assisted tunneling because accurate values for the electron-phonon matrix elements have been given only for the LA[16] phonon between states of symmetry Γ_2' and L_1. In this section, we shall make qualitative estimates of the phonon-assisted tunneling due to TA, LO, and TO phonon emission.

The strength of the TA phonon-assisted tunneling (conductance change at $eV = \pm \hbar\omega_{TA}$) can be estimated if it is assumed that $M_{TA} = M_{LA}$ (as done, for example, in Reference 6) and if the important region for the electron-phonon interaction is near, but not in the Schottky-barrier region ($x > d$). Since a typical energy of the metal - Γ_2' states is $E_{\Gamma c} - E_{Lc} - e\mu_F$ below the Γ_2' conduction band edge, the Γ_2' tail contains some Γ_{25}' character. The magnitude of the Γ_{25}' admixture relative to Γ_2' is approximately $(E_{\Gamma c} - E_{Lc} - e\mu_F)/Eg \simeq 0.14$. ($E_g$ is the direct gap at $\underline{k} = 0$.) Since the $\Gamma_{25}' \leftrightarrow L_1$ transition is allowed for TA phonons (see Fig. 5) and there are 2 transverse phonon branches, the change in conductance at $eV = \pm \hbar\omega_{TA}$ should be about 2 x .14 or $\sim$ 30% of that at $eV = \pm \hbar\omega_{LA}$. From Fig. 4, we see that this rough estimate is reasonable. We have neglected the contribution from the electron-phonon interaction in the Schottky-barrier region ($0<x<d$) and have neglected the contribution from the admixture of L_3' into the L_1 conduction band states, which is $\sim e\mu_F/(E_{Lc}-E_{Lv}) \approx 10^{-2}$. ($E_{Lc} - E_{Lv}$ is the energy gap between L_1 and L_3'.) The allowed transition $\Gamma_2' \leftrightarrow L_3'$ should therefore contribute to the TA phonon-assisted tunneling only $\sim$ 1% as much as the $\Gamma_{25}' \leftrightarrow L_1$ if the relevant matrix elements are comparable.

The strength of the LO phonon-assisted tunneling can be compared to the strength of the TA phonon-assisted tunneling since the $\Gamma_{25}' \leftrightarrow L_1$ transition is

allowed for both LO and TA phonons (Fig. 5). If the matrix element for LO phonon emission is the same as for TA phonon emission, then the change in conductance at $eV = \pm \hbar\omega_{LO}$ should be about half of that at $eV = \pm \hbar\omega_{TA}$ since there is only one longitudinal branch. This rough estimate is also in reasonable agreement with the experimental results (Fig. 4). (As before, we neglect the LO contribution from the $\Gamma_2' \leftrightarrow L_3'$ transition ($\sim$1%).)

The estimated relative strengths of the TO and the LO phonon-assisted tunneling is, however, not in good agreement with the experimental results. The allowed transition for TO phonons is $\Gamma_{25}' \leftrightarrow L_3'$, whereas the allowed transition for LO phonons is $\Gamma_{25}' \leftrightarrow L_1$ (Fig. 5). If the matrix elements for these two transitions are comparable, we would expect the relative strengths of TO to LO to be $2\, e\mu_F/(E_{Lc} - E_{Lv})$, or $\sim$ 2%. From Fig. 5, we see that the experimental data show that the TO phonon-assisted tunneling is comparable to the LO phonon-assisted tunneling, not 50 times smaller. We are, therefore, forced to conclude that either the TO matrix element is nearly an order of magnitude larger than the LO matrix element, or that the TO phonon-assisted tunneling proceeds by a mechanism which does not obey the selection rules, such as scattering from crystal imperfections.

VI. Summary

One group of metal-Ge (n-type) tunnel junctions studied in this investigation were fabricated by cleaving Ge crystals in vacuum and then evaporating metal electrodes (In or Pb) through a metal mask onto the cleaved surface. For junctions which were made from Sb-doped Ge ($n \simeq 7 \times 10^{18}$ cm^{-3}), it was found that the experimentally measured conductance vs bias voltage curves agreed in shape and magnitude with the predictions of the one-electron Schottky-barrier[1]

model where all parameters were determined from experiments other than tunneling.

Such agreement, although somewhat fortuitous, showed that the following approximations or assumptions are adequate in the description of these tunnel junctions. (1) The electrostatic potential near the metal-semiconductor interface can be replaced by an average, parabolic potential. (2) Specular reflection occurs at the interface. (3) The energy levels of the highly doped, degenerate n-type Ge are given by $\frac{\hbar^2 k^2}{2m_c^*}$ (or an appropriate generalization for ellipsoidal energy surfaces) and that at $T = 0^{\circ}K$ these states are filled up to $e\mu_F$ above the conduction band edge.

The conductance curves for vacuum-cleaved As-doped units do not agree with theory in magnitude as well as the Sb-doped units, but the qualitative features are similar. This discrepancy is not understood at present.

Capacitance measurements have been made on both vacuum-cleaved and air-cleaved junctions. For vacuum-cleaved units, the barrier height was found to be $V_b = 0.63$ V and for air-cleaved, $V_b = 0.51$ V. A substantially higher conductance due to the lower barrier height was observed in the air-cleaved junctions which formed the second group of junctions studied. The measured barrier heights were independent of the contact metal (In or Pb) and of the semiconductor impurity (Sb or As).

Strong phonon-assisted tunneling was observed in both Sb-doped and As-doped vacuum-cleaved units. Air-cleaved units showed only weak phonon-assisted tunneling. Prominent step increases in the conductance of vacuum-cleaved junctions were observed at bias $eV = \pm \hbar\omega$, where $\hbar\omega$ is the energy of a Ge zone-boundary phonon along the <111> direction. Structure associated with the LA phonon was the strongest. The TA phonon structure was not as strong as that

for the LA phonons. The structure for the LO and the TO phonons was somewhat weaker than the structure for the acoustic phonons, but still clearly observable in dI/dV.

A calculation of the LA phonon-assisted tunneling has been presented in Sec. 4. The predicted strength of the step increases in the conductance at $eV = \pm \hbar\omega_{LA}$ is of the same order of magnitude as that observed experimentally. The calculation is based upon a modification of Kleinman's[6] explanation of similar phenomena in Ge p-n junctions. The essential feature of the mechanism is a two-step process, where (in reverse bias), an electron is injected from the metal into an evanescent semiconductor state associated with the Γ_2' conduction band and then emits a LA phonon with $\underline{q} \simeq \frac{-\pi}{a}(1, 1, 1)$, making a transition to a current carrying state at L_1. A similar process occurs at forward bias. Since this is an inelastic emission process, the conductance has a symmetric (with respect to zero-bias) threshold characteristic which is clearly seen in the experimental data.

A qualitative analysis of the phonon-assisted tunneling due to TA, LO, and TO phonon emission has been given in Sec. 5. The relative strengths of the conductance changes at $eV = \pm \hbar\omega$ ($\omega = \omega_{TA}$, ω_{LO}, or ω_{TO}) were found to be reasonable for TA and LO phonons assuming the appropriate electron-phonon matrix elements are comparable. The strength of the TO phonon emission, however, is experimentally nearly 50 times larger than expected. This strong TO phonon-assisted tunneling is not understood.

It should be pointed out that the mechanism for phonon-assisted tunneling described in this paper (with the possible exception of the TO phonons), is due

to the coherent coupling of the tunneling electrons to the constituent atoms of the semiconductor electrode and is not due to incoherent, impurity-induced coupling.[18]

Finally, it should be noted that the sharp, strong structure in d^2I/dV^2 at $eV = \pm \hbar\omega$ provides an accurate method of measuring the phonon energies. The pronounced minimum in the conductance at $V = \mu_F$ gives a reasonable estimate of the Fermi degeneracy. So the metal-semiconductor tunnel junction prepared by the vacuum-cleavage technique provides a useful spectrographic tool.[3]

Acknowledgments

The authors would like to acknowledge Miss L. Roth of Purdue University for the supply of Sb-doped samples, Professor C. T. Sah for the use of an rf admittance bridge, and Professors W. D. Compton and C. B. Duke for useful discussions.

References

1. J. W. Conley, C. B. Duke, G. D. Mahan, and J. J. Tiemann, Phys. Rev. 150, 466 (1966).

2. J. W. Conley and J. J. Tiemann, J. Appl. Phys. 38, 2880 (1967).

3. F. Steinrisser, L. C. Davis, and C. B. Duke, Phys. Rev. 176, 912 (1968).

4. R. T. Payne, Phys. Rev. 139, A570 (1965), (Additional references can be found in this reference.)

5. H. Holonyak, Jr., I. A. Lesk, R. N. Hall, J. J. Tiemann, and H. Ehrenreich, Phys. Rev. Letters 3, 167 (1959).

6. L. Kleinman, Phys. Rev. 140, A637 (1965).

7. We are indebted to E. L. Wolf for discussing this technique.

8. J. G. Adler and J. E. Jackson, Rev. Sci. Insts. 37, 1049 (1966).

9. J. W. Conley and G. D. Mahan, Phys. Rev. 161, 681 (1967). Eq. (4.1) of this reference contains a typographical error. Eq. (2.3) of this paper is the correct result.

10. W. G. Spitzer, F. A. Trumbore, and R. A. Logan, J. Appl. Phys. 32, 1822 (1961).

11. In Fig. 1 of Reference 3, a value of $7.5 \times 10^{18}/cm^3$ had been assumed from resistivity measurements. The new value of $6.7 \times 10^{18}/cm^3$ was obtained from Hall measurements on the tunneling sample.

12. J. J. Tiemann and H. Fritzsche, Phys. Rev. 137, A1910 (1965). M. Lax and J. J. Hopfield, Phys. Rev. 124, 115 (1961).

13. J. M. Luttinger and W. Kohn, Phys. Rev. 97, 869 (1955). (Additional references can be found in this reference.)

14. D. J. BenDaniel and C. B. Duke, Phys. Rev. 152, 683 (1966).

15. J. C. P. Miller in "Handbook of Mathematical Functions," edited by M. Abramowitz and I. A. Stegun (U. S. Department of Commerce, National Bureau of Standards, Washington, D. C., 1964), Appl. Math. Ser. 55, p. 685.

References - continued

16. Values of the parameters can be found in Reference 6 and Reference 12. The phonon energy $\hbar\omega_{LA}$ has been accurately measured by R. T. Payne, Reference 4. The value for M^2_{LA} is due to E. O. Kane, J. Appl. Phys. 32, 83 (1961), who analyzed the optical adsorption data of Reference 17. Typical values of v_F can be found in W. J. Tomasch, Phys. Rev. Letters 16, 16, 1966. The separation $E_{\Gamma c} - E_{Lc}$ has been measured by Conley and Tiemann, Reference 2.

17. G. G. Macfarlane, T. P. McLean, J. E. Quarrington, and V. Roberts, Phys. Rev. 108, 1377 (1957)

18. C. B. Duke, S. D. Silverstein, and A. J. Bennett, Phys. Rev. Letters 19, 312 (1967), Phys. Rev. 176, 969 (1968).

Figure Captions

Fig. 1 Schematic drawing of the circuit used to measure dI/dV and d^2I/dV^2.

Fig. 2 Comparison between experimental conductance vs voltage curve (solid line) on $n_D = 6.7 \times 10^{18}/cm^3$ Sb-doped Ge at 4.2^oK and the conductance calculated according to the model developed in Reference 8 (dashed line). The contact metal is In. The contact area is 2.5×10^{-4} cm^2, and the barrier height is 0.63 V. The Fermi degeneracy $\mu_F = 23$ mV.

Fig. 3 Comparison between experimental conductance vs voltage curves (solid lines) on As-doped Ge at 4.2^oK and the conductance calculated using the model developed in Reference 8 (dashed lines) with In as the contact metal. The lower curves represent a vacuum-cleaved sample for which the barrier height $V_b = 0.63$ V. The upper curves represent an air-cleaved sample with $V_b = 0.51$ V. Doping level and junction area for both samples are $7.0 \times 10^{18}/cm^3$ and 2.5×10^{-4} cm^2, respectively. The Fermi degeneracy $\mu_F = 24$ mV.

Fig. 4 Conductance and d^2I/dV^2 of an indium contact on As-doped Ge junction at 2^oK. The arsenic doping concentration is $n_D = 5.1 \times 10^{18}/cm^3$. The observation of the In superconducting gap at zero bias is shown explicitly. Its presence shifts the phonon structure to higher energies by $\Delta = 0.5$ mV. Assignment of phonon energies is according to Reference 4. Sign convention for bias voltage is opposite to that of Reference 3.

Figure Captions - continued

Fig. 5 Simplified model of the band structure for Ge and allowed phonon-assisted transitions between the band extreme (see Reference 12).

Fig. 6 (a) Schematic representation of metal-Ge (n-type) interface in $\underline{k}$-space. One-electron tunneling flows via direct channel. Phonon-assisted tunneling involves two-step process. For reverse bias, step 1 is the injection of an electron from the metal Fermi surface into an evanescent semiconductor state associated with the Γ_2' conduction band. Step 2 is the emission of a Ge phonon of momentum $\underline{q} \simeq \frac{-\pi}{a}(1, 1, 1)$ and the transition of the electron to a current-carrying state in the L_1 conduction band. A similar process occurs in forward bias. (b) The metal - Γ_2' envelope function. Metal wavefunction connects onto an evanescent semiconductor state associated with Γ_2' conduction band.

Fig. 7 The component of the conductance due to LA phonon-assisted tunneling.

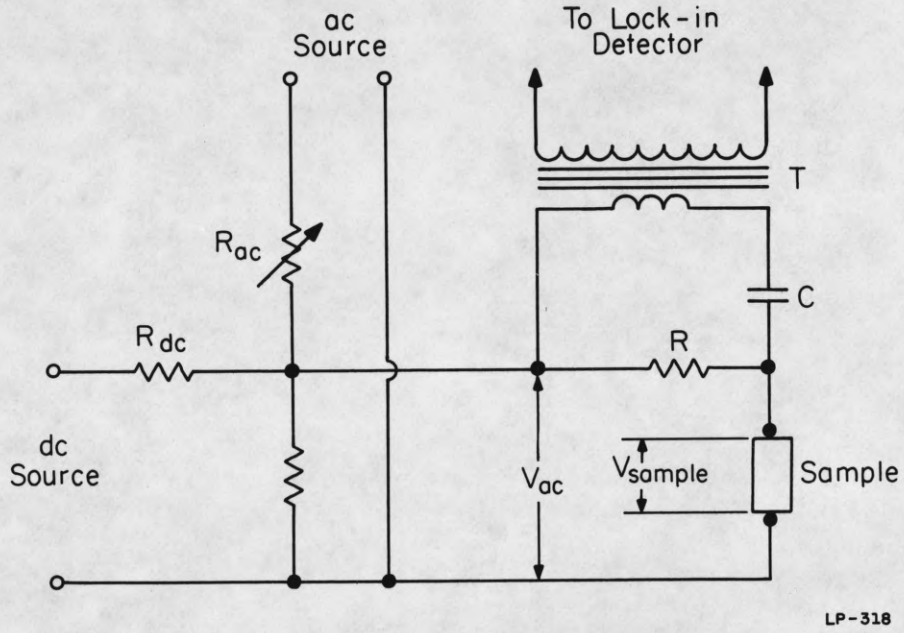
ac
Source
To Lock-in
Detector
T
C
R_{ac}
R_{dc}
R
dc
Source
V_{ac}
V_{sample}
Sample
LP-318

Figure 1

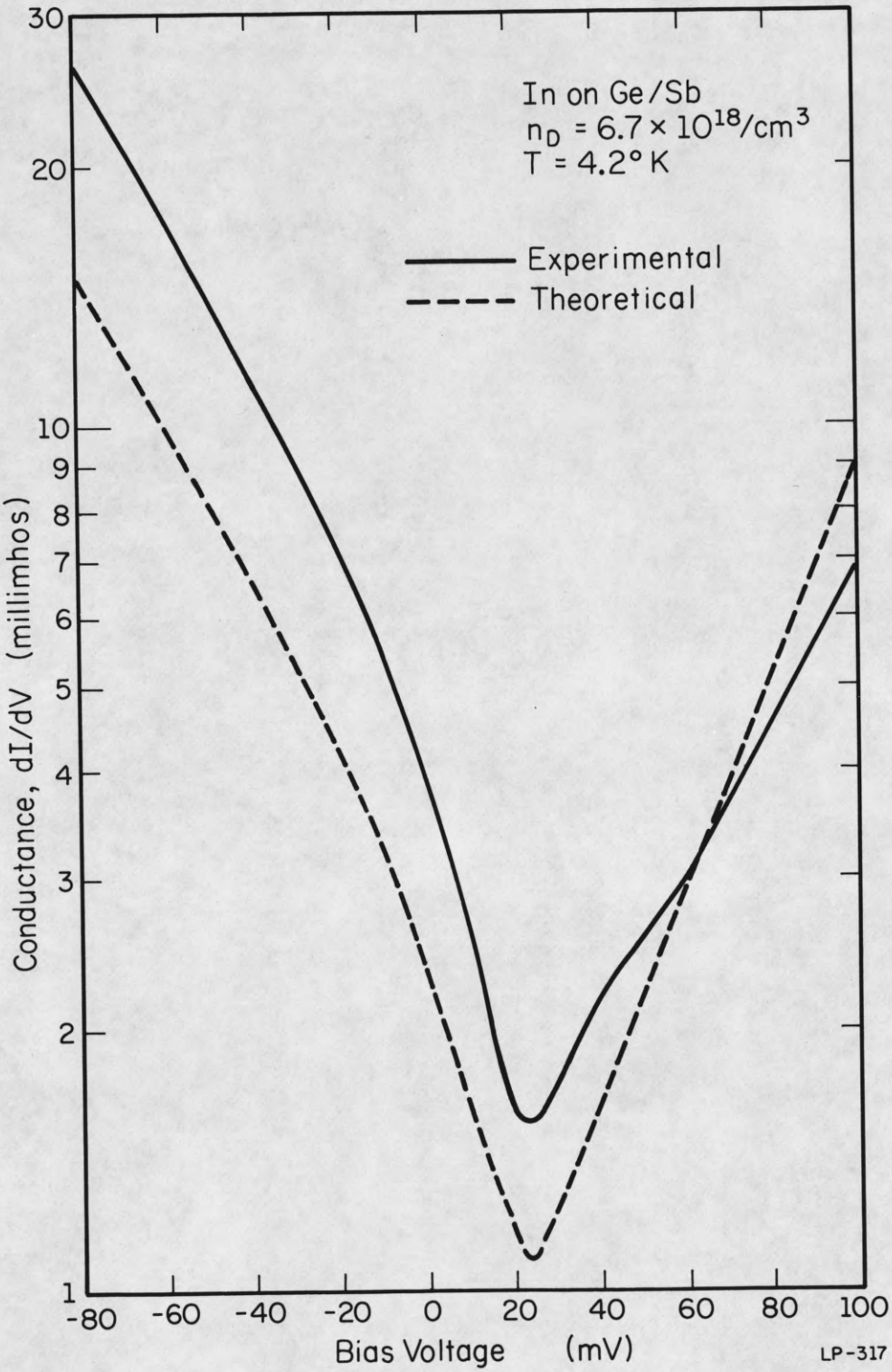
In on Ge/Sb
$n_D = 6.7 \times 10^{18}/cm^3$
T = 4.2° K
Experimental
Theoretical
Conductance, dI/dV (millimhos)
30
20
10
9
8
7
6
5
4
3
2
1
-80
-60
-40
-20
0
20
40
60
80
100
Bias Voltage (mV)
LP-317

Figure 2

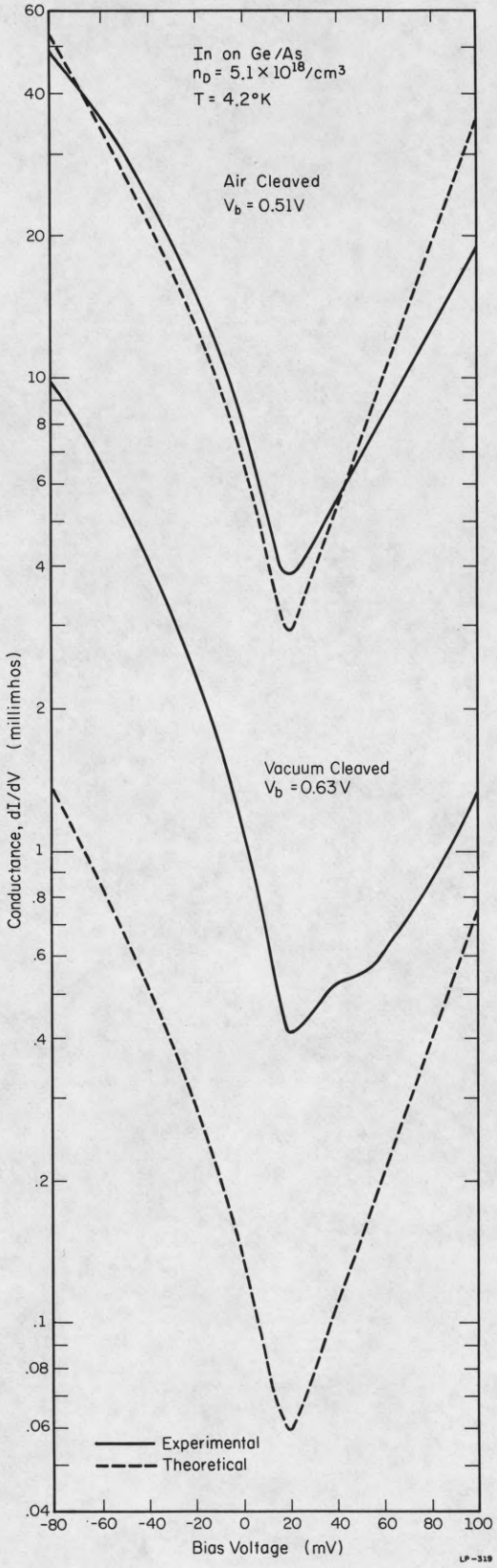
In on Ge/As
$n_D = 5.1 \times 10^{18}/cm^3$
T = 4.2°K
Air Cleaved
V_b = 0.51V
Vacuum Cleaved
V_b = 0.63V
Experimental
Theoretical
Conductance, dI/dV (millimhos)
Bias Voltage (mV)
60
40
20
10
8
6
4
2
1
.8
.6
.4
.2
.1
.08
.06
.04
-80
-60
-40
-20
0
20
40
60
80
100
LP-319

Figure 3

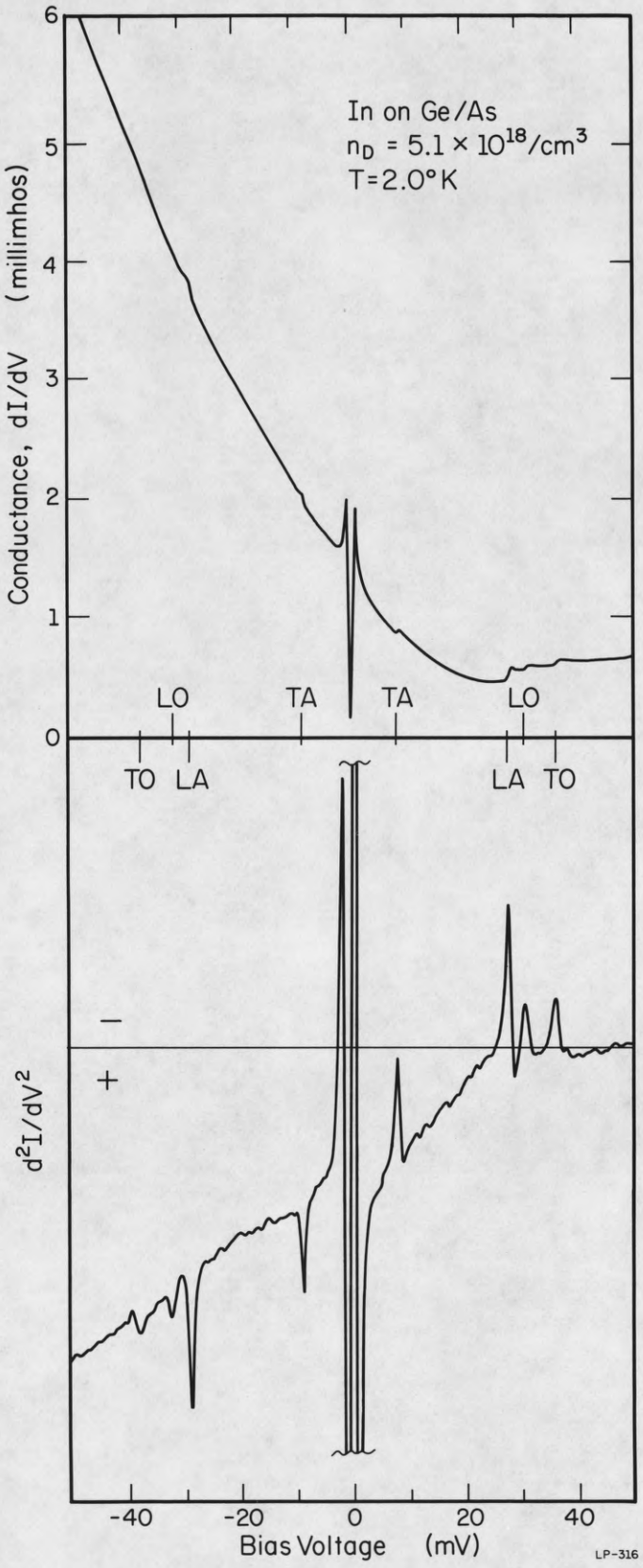
In on Ge/As
$n_D = 5.1 \times 10^{18}/cm^3$
T=2.0°K
Conductance, dI/dV (millimhos)
6
5
4
3
2
1
0
LO
TA
TA
LO
TO
LA
LA
TO
−
+
d^2I/dV^2
-40
-20
0
20
40
Bias Voltage (mV)
LP-316

Figure 4

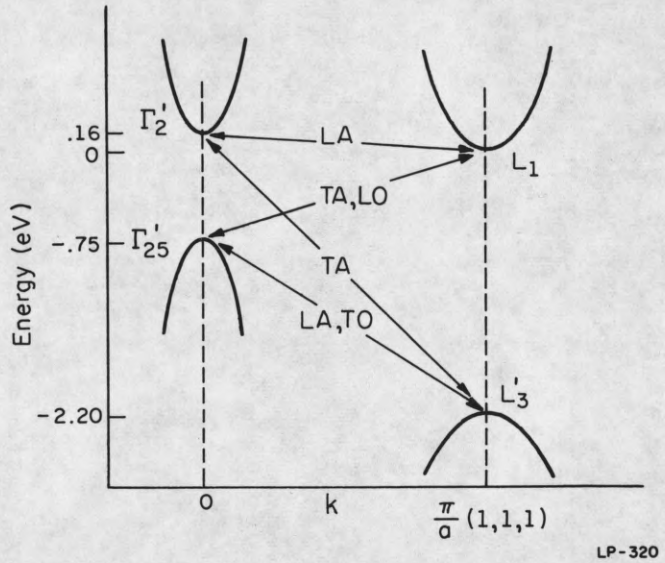
Energy (eV)
.16
0
-.75
-2.20
Γ_2'
Γ_{25}'
LA
TA,LO
TA
LA,TO
L_1
L_3'
0
k
$\frac{\pi}{a}$(1,1,1)
LP-320

Figure 5

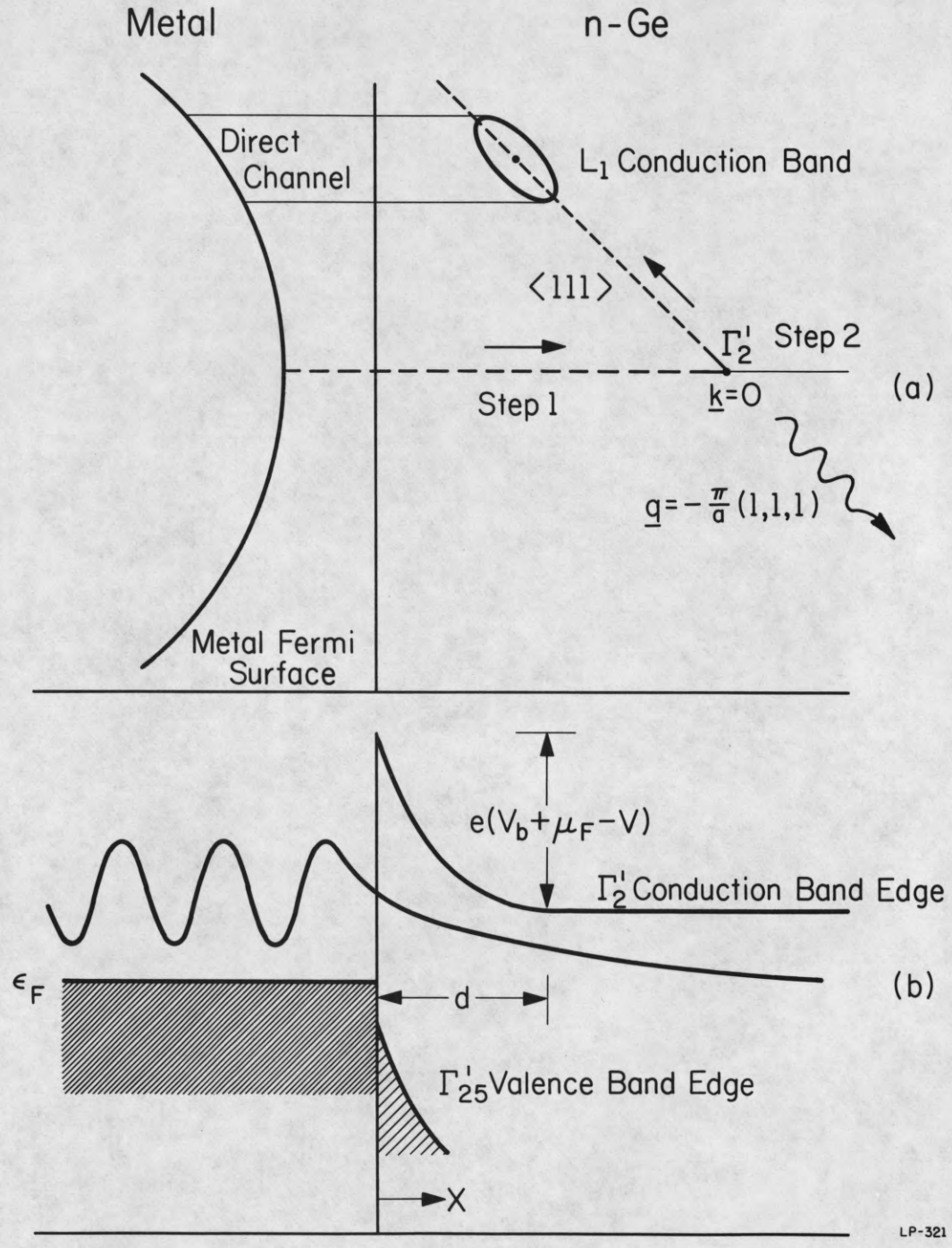
Metal
n-Ge
Direct Channel
L_1 Conduction Band
⟨111⟩
Γ_2' Step 2
Step 1
$\underline{k}=0$
(a)
$\underline{q}=-\frac{\pi}{a}(1,1,1)$
Metal Fermi Surface
$e(V_b+\mu_F-V)$
Γ_2' Conduction Band Edge
ϵ_F
d
(b)
Γ_{25}' Valence Band Edge
X
LP-321

Figure 6

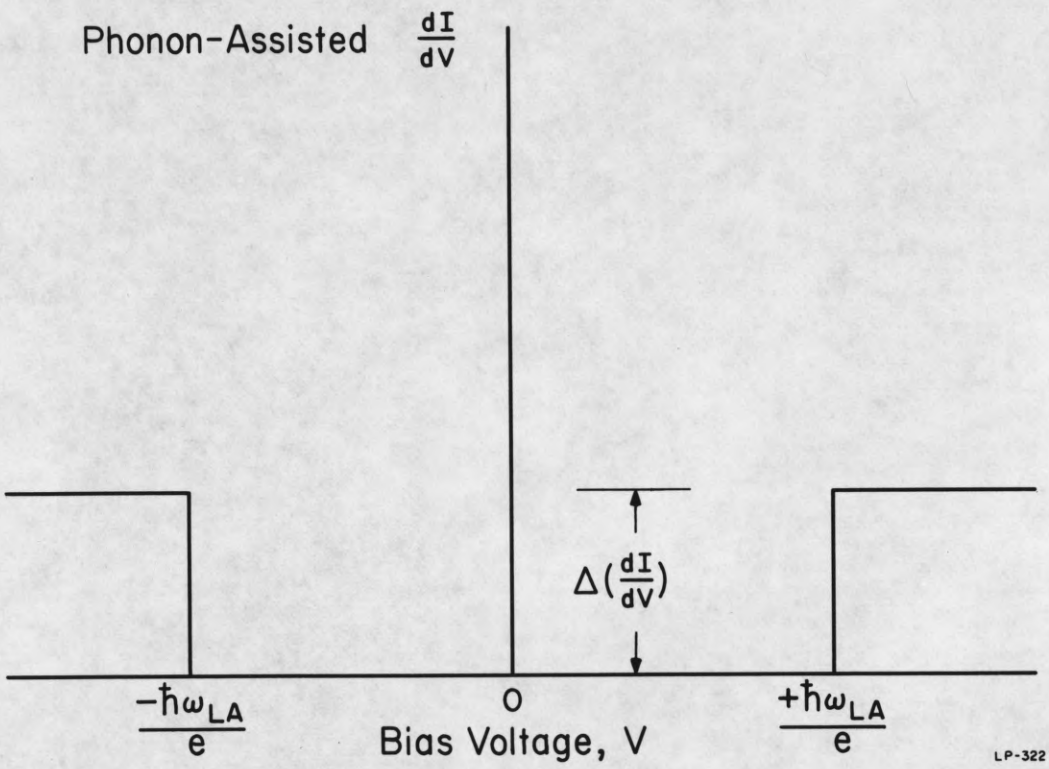
Phonon-Assisted
dI/dV
Δ(dI/dV)
−ħω_LA/e
0
+ħω_LA/e
Bias Voltage, V
LP-322

Figure 7

Distribution List as of April 1, 1969

Dr A.A. Dougal
Asst Director (Research)
Ofc of Defense Res & Eng
Department of Defense
Washington, D.C. 20301

Office of Deputy Director
(Research and Information, Rm 3D1037)
Department of Defense
The Pentagon
Washington, D.C. 20301

Director, Advanced Research Projects
Agency
Department of Defense
Washington, D.C. 20301

Director for Materials Sciences
Advanced Research Projects Agency
Department of Defense
Washington, D.C. 20301

Headquarters
Defense Communications Agency (340)
Washington, D.C. 20305

Defense Documentation Center
Attn: DDC-TCA
Cameron Station
Alexandria, Virginia 22314 (50 Copies)

Director
National Security Agency
Attn: TDL
Fort George G. Meade, Maryland 20755

Weapons Systems Evaluation Group
Attn: Colonel Blaine O. Vogt
400 Army-Navy Drive
Arlington, Virginia 22202

Central Intelligence Agency
Attn: OCR/DD Publications
Washington, D.C. 20505

Hq USAF (AFRDD)
The Pentagon
Washington, D.C. 20330

Hq USAF (AFRDDG)
The Pentagon
Washington, D.C. 20330

Hq USAF (AFRDSD)
The Pentagon
Washington, D.C. 20330

Colonel E.P. Gaines, Jr.
ACDA/FO
1901 Pennsylvania Ave N.W.
Washington, D.C. 20451

Lt Col R.B. Kalisch (SREE)
Chief, Electronics Division
Directorate of Engineering Sciences
Air Force Office of Scientific Research
Arlington, Virginia 22209

Dr I.R. Mirman
AFSC (SCT)
Andrews Air Force Base, Maryland 20331

AFSC (SCTSE)
Andrews Air Force Base, Maryland 20331

Mr Morton M. Pavane, Chief
AFSC Scientific and Technical Liaison Office
26 Federal Plaza, Suite 1313
New York, New York 10007

Rome Air Development Center
Attn: Documents Library (EMTLD)
Griffiss Air Force Base, New York 13440

Mr H.E. Webb (EMMIIS)
Rome Air Development Center
Griffiss Air Force Base, New York 13440

Dr L.M. Hollingsworth
AFCRL (CRN)
L.G. Hanscom Field
Bedford, Massachusetts 01730

AFCRL (CRMPLR), Stop 29
AFCRL Research Library
L.G. Hanscom Field
Bedford, Massachusetts 01730

Hq ESD (ESTI)
L.G. Hanscom Field
Bedford, Massachusetts 01730 (2 copies)

Professor J. J. D'Azzo
Dept of Electrical Engineering
Air Force Institute of Technology
Wright-Patterson AFB, Ohio 45433

Dr H.V. Noble (CAVT)
Air Force Avionics Laboratory
Wright-Patterson AFB, Ohio 45433

Director
Air Force Avionics Laboratory
Wright-Patterson AFB, Ohio 45433

AFAL (AVTA/R.D. Larson
Wright-Patterson AFB, Ohio 45433

Director of Faculty Research
Department of the Air Force
U.S. Air Force Academy
Colorado Springs, Colorado 80840

Academy Library (DFSLB)
USAF Academy
Colorado Springs, Colorado 80840

Director
Aerospace Mechanics Division
Frank J. Seiler Research Laboratory (OAR)
USAF Academy
Colorado Springs Colorado 80840

Director, USAF PROJECT RAND
Via: Air Force Liaison Office
The RAND Corporation
Attn: Library D
1700 Main Street
Santa Monica, California 90045

Hq SAMSO (SMTTA/Lt Nelson)
AF Unit Post Office
Los Angeles, California 90045

Det 6, Hq OAR
Air Force Unit Post Office
Los Angeles, California 90045

AUL3T-9663
Maxwell AFB, Alabama 36112

AFETR Technical Library
(ETV,MU-135)
Patrick AFB,Florida 32925

ADTC (ADBPS-12)
Eglin AFB, Florida 32542

Mr B.R. Locke
Technical Adviser, Requirements
USAF Security Service
Kelly Air Force Base, Texas 78241

Hq AMD (AMR)
Brooks AFB, Texas 78235

USAFSAM (SMKOR)
Brooks AFB, Texas 78235

Commanding General
Attn: STEWS-RE-L, Technical Library
White Sands Missile Range
New Mexico 88002 (2 copies)

Hq AEDC (AETS)
Attn: Library/Documents
Arnold AFS, Tennessee 37389

European Office of Aerospace Research
APO New York 09667

Physical & Engineering Sciences Division
U.S. Army Research Office
3045 Columbia Pike
Arlington, Virginia 22204

Commanding General
U.S. Army Security Agency
Attn: IARD-T
Arlington Hall Station
Arlington, Virginia 22212

Commanding General
U.S. Army Materiel Command
Attn: AMCRD-TP
Washington, D.C. 20315

Technical Director (SMUFA-A2000-107-1)
Frankford Arsenal
Philadelphia, Pennsylvania 19137

Redstone Scientific Information Center
Attn: Chief, Document Section
U.S. Army Missile Command
Redstone Arsenal, Alabama 35809

Commanding General
U.S. Army Missile Command
Attn: AMSMI-REX
Redstone Arsenal, Alabama 35809

Commanding General
U.S. Army Strategic Communications Command
Attn: SCC-CG-SAE
Fort Huachuca, Arizona 85613

Commanding Officer
Army Materials and Mechanics Res. Center
Attn: Dr H. Priest
Watertown Arsenal
Watertown, Massachusetts 02172

Commandant
U.S. Army Air Defense School
Attn: Missile Science Division, C&S Dept
P.O. Box 9390
Fort Bliss, Texas 79916

Commandant
U.S. Army Command & General Staff College
Attn: Acquisitions, Library Division
Fort Leavenworth, Kansas 66027

Commanding Officer
U.S. Army Electronics R&D Activity
White Sands Missile Range, New Mexico 88002

Mr Norman J. Field, AMSEL-RD-S
Chief, Office of Science & Technology
Research and Development Directorate
U.S. Army Electronics Command
Fort Monmouth, New Jersey 07703

Commanding Officer
Harry Diamond Laboratories
Attn: Dr Berthold Altman (AMXDO-TI)
Connecticut Avenue and Van Ness St N.W.
Washington, D.C. 20438

Director
Walter Reed Army Institute of Research
Walter Reed Army Medical Center
Washington, D.C. 20012

Commanding Officer (AMXRD-BAT)
U.S. Army Ballistics Research Laboratory
Aberdeen Proving Ground
Aberdeen, Maryland 21005

Technical Director
U.S. Army Limited War Laboratory
Aberdeen Proving Ground
Aberdeen, Maryland 21005

Commanding Officer
Human Engineering Laboratories
Aberdeen Proving Ground
Aberdeen, Maryland 21005

U.S. Army Munitions Command
Attn: Science & Technology Br. Bldg 59
Picatinny Arsenal, SMUPA-VA6
Dover, New Jersey 07801

U.S. Army Mobility Equipment Research
and Development Center
Attn: Technical Document Center, Bldg 315
Fort Belvoir, Virginia 22060

Director
U.S. Army Engineer Geodesy,
Intelligence & Mapping
Research and Development Agency
Fort Belvoir, Virginia 22060

Dr Herman Robl
Deputy Chief Scientist
U.S. Army Research Office (Durham)
Box CM, Duke Station
Durham, North Carolina 27706

Richard O. Ulsh (CRDARD-IPO)
U.S. Army Research Office (Durham)
Box CM, Duke Station
Durham, North Carolina 27706

Mr Robert O. Parker, AMSEL-RD-S
Executive Secretary, JSTAC
U.S. Army Electronics Command
Fort Monmouth, New Jersey 07703

Commanding General
U.S. Army Electronics Command
Fort Monmouth, New Jersey 07703

Attention:AMSEL-SC
RD-GF
RD-MT
XL-D
XL-E
XL-C
XL-S (Dr R. Buser)
HL-CT-DD
HL-CT-R
HL-CT-L (Dr W.S. McAfee)
HL-CT-O
HL-CT-I
HL-CT-A
NL-D
NL-A
NL-P
NL-P-2 (Mr D. Haratz)
NL-R (Mr R. Kulinyi)
NL-S
KL-D
KL-E
KL-S (Dr H. Jacobs)
KL-SM (Drs Schiel/Hieslmair)
KL-T
VL-D
VL-F (Mr R.J. Niemela)
WL-D

1 copy to each symbol listed individually addressed

Dr A.D. Schnitzler, AMSEL-HL-NVII
Night Vision Laboratory, USAECOM
Fort Belvoir, Virginia 22060

Dr G.M. Janney, AMSEL-HL-NVOR
Night Vison Laboratory,USAECOM
Fort Belvoir, Virginia 22060

Atmospheric Sciences Office
Atmospheric Sciences Laboratory
White Sands Missile Range
New Mexico 88002

Missile Electronic Warfare,
Technical Area, AMSEL-WT-MT
White Sands Missile Range
New Mexico 88002

Project Manager
Commcn Positioning & Navigation Systems
Attn: Harold H. Bahr (AMCPM-NS-TM), Bldg 439
U.S. Army Electronics Command
Fort Monmouth, New Jersey 07703

Director, Electronic Programs
Attn: Code 427
Department of the Navy
Washington, D.C. 20360

Commander
U.S. Naval Security Group Command
Attn: G43
3801 Nebraska Avenue
Washington, D.C. 20390

Director
Naval Research Laboratory
Washington, D.C. 20390
Attn: Code 2027 6 copies
Dr W.C. Hall, Code 7000 1 copy
Dr A. Brodizinsky, Sup.Elec Div. 1 copy

Dr G.M.R. Winkler
Director, Time Service Division
U.S. Naval Observatory
Washington, D.C. 20390

Naval Air Systems Command
AIR 03
Washington, D.C. 20360 2 copies

Naval Ship Systems Command
Ship 031
Washington, D.C. 20360

Naval ship Systems Command
Ship 035
Washington, D.C. 20360

U.S. Naval Weapons Laboratory
Dahlgren, Virginia 22448

Naval Electronic Systems Command
ELEX 03, Room 2046 Munitions Building
Department of the Navy
Washington, D.C. 20360 (2 copies)

Commander
Naval Electronics Laboratory Center
Attn: Library
San Diego, California 92152 (2 copies)

Deputy Director and Chief Scientist
Office of Naval Research Branch Office
1030 Est Gree Street
Pasadena, California 91101

Library (Code2124)
Technical Report Section
Naval Postgraduate School
Monterey, California 93940

Glen A. Myers (Code 52Mv)
Assoc Professor of Elec. Engineering
Naval Postgraduate School
Monterey, California 93940

Commanding Officer and Director
U.S. Naval Underwater Sound Laboratory
Fort Trumbull
New London, Connecticut 06840

Commanding Officer
Naval Avionics Facility
Indianapolis, Indiana 46241

Dr H. Harrison, Code RRE
Chief, Electrophysics Branch
National Aeronautics & Space Admin.
Washington, D.C. 20546

NASA Lewis Research Center
Attn: Library
21000 Brookpark Road
Cleveland, Ohio 44135

Los Alamos Scientific Laboratory
Attn: Report Library
P.O. Box 1663
Los Alamos, New Mexico 87544

Federal Aviation Administration
Attn: Admin Stds Div (MS-110)
800 Independence Ave S.W.
Washington, D.C. 20590

Head, Technical Services Division
Naval Investigative Service Headquarters
4420 North Fairfax Drive
Arlington, Virginia 22203

Commander
U.S. Naval Ordnance Laboratory
Attn: Librarian
White Oak, Maryland 21502 (2 copies)

Commanding Officer
Office of Naval Research Branch Office
Box 39 FPO
New York, New York 09510

Commanding Officer
Office of Naval Research Branch Office
219 South Dearborn Street
Chicago, Illinois 60604

Commanding Officer
Office of Naval Research Branch Office
495 Summer Street
Boston, Massachusetts 02210

Commander (ADL)
Naval Air Development Center
Johnsville, Warminster, Pa 18974

Commanding Officer
Naval Training Device Center
Orlando, Florida 32813

Commander (Code 753)
Naval Weapons Center
Attn: Technical Library
China Lake, California 93555

Commanding Officer
Naval Weapons Center
Corona Laboratories
Attn: Library
Corona, California 91720

Commander, U.S. Naval Missile Center
Point Mugu, California 93041

W.A. Eberspacher, Associate Head
Systems Integration Division
Code 5340A, Box 15
U.S. Naval Missile Center
Point Mugu, California 93041

Mr M. Zane Thornton, Chief
Network Engineering, Communications
and Operations Branch
Lister Hill National Center for
Biomedical Communications
8600 Rockville Pike
Bethesda, Maryland 20014

U.S. Post Office Department
Library - Room 1012
12th & Pennsylvania Ave, N.W.
Washington, D.C. 20260

Director
Research Laboratory of Electronics
Massachusetts Institute of Technology
Cambridge, Massachusetts 02139

Mr Jerome Fox, Research Coordinator
Polytechnic Institute of Brooklyn
55 Johnson Street
Brooklyn, New York 11201

Director
Columbia Radiation Laboratory
Columbia University
538 West 120th Street
New York, New York 10027

Director
Coordinated Science Laboratory
University of Illinois
Urbana, Illinois 61801

Director
Stanford Electronics Laboratories
Stanford University
Stanford, California 94305

Director
Microwave Physics Laboratory
Stanford University
Stanford, California 94305

Director, Electronics Research Laboratory
University of California
Berkeley, California 94720

Director
Electronic Sciences Laboratory
University of Southern California
Los Angeles, California 90007

Director
Electronics Research Center
The University of Texas at Austin
Austin Texas 78712

Division of Engineering and Applied Physics
210 Pierce Hall
Harvard University
Cambridge, Massachusetts 02138

Dr G.J. Murphy
The Technological Institute
Northwestern University
Evanston, Illinois 60201

Dr John C. Hancock, Head
School of Electrical Engineering
Purdue University
Lafayette, Indiana 47907

Dept of Electrical Engineering
Texas Technological College
Lubbock, Texas 79409

Aerospace Corporation
P.O. Box 95085
Los Angeles, California 90045
Attn: Library Acquisitions Group

Proffessor Nicholas George
California Inst of Technology
Pasadena, California 91109

Aeronautics Library
Graduat Aeronautical Laboratories
California Institute of Technology
1201 E. California Blvd
Pasadena, California 91109

The John Hoplins University
Applied Physics Laboratory
Attn: Document Librarian
8621 Georgia Avenue
Silver Spring, Maryland 20910

Raytheon Company
Attn: Librarian
Bedford, Massachusetts 01730

Raytheon Company
Research Division Library
28 Seyon Street
Waltham, Massachusetts 02154

Dr Sheldon J. Wells
Electronic Properties Information Center
Mail Station E-175
Hughes Aircraft Company
Culver City, California 90230

Dr Robert E. Fontana
Systems Research Laboratories Inc.
7001 Indian Ripple Road
Dayton, Ohio 45440

Nuclear Instrumentation Group
Bldg 29, Room 101
Lawrence Radiation Laboratory
University of California
Berkeley, California 94720

Sylvania Electronic Systems
Applied Research Laboratory
Attn: Documents Librarian
40 Sylvan Road
Waltham, Massachusetts 02154

Hollander Associates
P.O. Box 2276
Fullerton, California 92633

Illinois Institute of Technology
Dept of Electrical Engineering
Chicago, Illinois 60616

The University of Arizona
Dept of Electrical Engineering
Tucson, Arizona 85721

Utah State University
Dept Of Electrical Engineering
Logan, Utah 84321

Case Institute of Technology
Engineering Division
University Circle
Cleveland, Ohio 44106

Hunt Library
Carnegie-Mellon University
Schenley Park
Pittsburgh, Pennsylvania 15213

Dr Leo Youns
Stanford Research Institute
Menlo Park, California 94025

School of Engineering Sciences
Arizona State University
Tempe, Arizona 85281

Engineering & Mathmatical Sciences Library
University of California at Los Angeles
405 Hilgred Avenue
Los Angeles, California 90024

The Library
Government Publications Section
University of California
Santa Barbara, California 93106

Carnegie Institute of Technology
Electrical Engineering Department
Pittsburgh, Pennsylvania 15213

Professor Joseph E. Rowe
Chairman, Dept of Electrical Engineering
The University of Michigan
Ann Arbor, Michigan 48104

New York University
College of Engineering
New York, New York 10019

Syracuse University
Dept of Electrical Engineering
Syracuse, New York 13210

Yale University
Engineering Department
New Haven, Connecticut 06520

Airborne Instruments Laboratory
Deerpark, New York 11729

Raytheon Company
Attn: Librarian
Bedford, Massachusetts 01730

Lincoln Laboratory
Massachusetts Institute of Technology
Lexington, Massachusetts 02173

The University of Iowa
The University Libraries
Iowa City, Iowa 52240

Lenkurt Electric Co,Inc
1105 County Road
San Carlos, California 94070
Attn: Mr E.K. Peterson

Philco Ford Corporation
Communications & Electronics Div.
Union Meeting and Jolly Rods
Blue Bell, Pennsylvania 19422

Union Carbide Corporation
Electronic Division
P.O. Box 1209
Mountain View, California 94041

Electromagnetic Compatibility Analysis Center
(ECAC), Attn: ACLP
North Severn
Annapolis, Maryland 21402

Director
U. S. Army Advanced Materiel Concepts Agency
Washington, D.C. 20315

ADDENDUM

Dept of Electrical Engineering
Rice University
Houston, Texas 77001

Research Laboratories for the Eng. Sc.
School of Engineering & Applied Science
University of Virginia
Charlottesville, Virginia 22903

Dept of Electrical Engineering
College of Engineering & Technology
Ohio University
Athens, Ohio 45701

Project MAC
Document Room
Massachusetts Institute of Technology
545 Technology Square
Cambridge, Massachusetts 02139

Lehigh University
Dept of Electrical Engineering
Bethelehem, Pennsylvania 18015

ERRATUM

Mr Jerome Fox, Research Coordinator
Polytechnic Institute of Brooklyn
55 Johnson Street (Should be 333 Jay Street)
Brooklyn, N.Y. 11201

Security Classification

DOCUMENT CONTROL DATA - R & D

(Security classification of title, body of abstract and indexing annotation must be entered when the overall report is classified)

1. ORIGINATING ACTIVITY *(Corporate author)*
University of Illinois
Coordinated Science Laboratory
Urbana, Illinois 61801

2a. REPORT SECURITY CLASSIFICATION
Unclassified

2b. GROUP

3. REPORT TITLE

ONE-ELECTRON AND PHONON-ASSISTED TUNNELING IN N-Ge SCHOTTKY BARRIERS

4. DESCRIPTIVE NOTES *(Type of report and inclusive dates)*

5. AUTHOR(S) *(First name, middle initial, last name)*

DAVIS, L.C., Steinrisser F.

6. REPORT DATE	7a. TOTAL NO. OF PAGES	7b. NO. OF REFS
June, 1969	36	18

8a. CONTRACT OR GRANT NO.
DAAB-07-67-C-0199; DA-31-124-ARO(D)-114;
b. PROJECT NO. also NsG 228-62
c.
d.

9a. ORIGINATOR'S REPORT NUMBER(S)
R-419

9b. OTHER REPORT NO(S) *(Any other numbers that may be assigned this report)*

10. DISTRIBUTION STATEMENT

This document has been approved for public release and sale; its distribuion is unlimited.

11. SUPPLEMENTARY NOTES

12. SPONSORING MILITARY ACTIVITY
Joint Services Electronics Program
thru U.S. Army Electronics Command
Fort Monmouth, New Jersey 07703

13. ABSTRACT

The experimental tunneling conductance of metal-Ge contacts is compared to the predictions of the one-electron Schottky-barrier model in which all parameters are determined from experiments other than tunneling. Agreement is found in the magnitude and the shape of conductance vs bias curves for vacuum-cleaved, Sb-doped Ge units. The qualitative features of the As-doped units are also in agreement, but a discrepancy in magnitude exists. Substantially larger conductance is found in air-cleaved junctions than in vacuum- cleaved junctions. Capacitance measurements reveal that the barrier height for air-cleaved junctions is V_b=0.51V whereas V_b= 0.63V for vacuum-cleaved junctions. Pronounced step increases in the conductance due to phonon-assisted tunneling occur at $eV = \pm\hbar\omega$ where $\hbar\omega$ is the energy of a Ge phonon at the Brillouin zone boundary along the <111> direction. Structure is clearly observed at all four phonon energies (TA,LA,LO,TO). The magnitude of the LA phonon-assisted tunneling is accounted for in a theoretical calculation bases upon a mechanism suggested by Kleinman to explain similar phenomena in Ge p-n junctions. The strength of the TA and LO phonon-assisted tunneling also appear to be in reasonable agreement with qualitative considerations, but the observed TO phonon-assisted tunneling is stronger than expected.

DD FORM 1 NOV 65 1473

Security Classification

14 KEY WORDS	LINK A		LINK B		LINK C	
	ROLE	WT	ROLE	WT	ROLE	WT
Tunneling Germanium Semiconductors						